Automatic Maneuvering of Vessels with Power-Optimized Thrust Allocation

Dr. A Schubert *, N Eisenblätter, MSc, R Damerius, MSc, Prof. T Jeinsch
University of Rostock, Institute of Automation, Germany
*Corresponding author. Email: agnes.schubert@uni-rostock.de

Synopsis

Assisted and automated ship maneuvering can contribute to safer and cleaner port operations. Power consumption can be reduced by optimizing the thrust allocation to the available actuators. Within the established structure for guidance, navigation and control, thrust allocation belongs to the control module. Each controller mode requires an associated allocation that distributes the commanded forces at the controller output to the ship's actuators so that the desired motion is achieved. The allocation problem is formulated as a quadratic program. The paper focuses on a generic allocation approach for a vessel with a maximum of six actuator units. The method is explained using the specifications of the 52 *m* long research vessel *DENEB* and for the various phases of automatic port maneuvers in the area of German Naval Base Command Rostock-Warnemünde. The paper presents the results for dynamic positioning maneuvers with the real vessel under the influence of wind using the developed allocation approach.

Keywords: Consumption optimisation; Manoeuvring automation; Quadratic programming

1 Introduction

The introduction of assistance and automation functions in conventional shipping is motivated by a number of factors. These include saving fuel and emissions, avoiding collisions and the growing shortage of experienced nautical officers, which prompted Japan to launch the MEGURI project (Miyoshi and Ioki (2021)). At the same time, the challenges of navigating safely are increasing due to higher traffic volumes and ever-growing ship sizes (UNITED NATIONS (2019)). Assisted and automated ship maneuvering can also contribute to safer and cleaner port operations where combined precise and slow motions in three degrees of freedom are required, often using the full available propulsion power to compensate for the large influence of environmental forces on the ship (Schubert et al. (2024a)).

The presented approach follows the method of successive maneuver automation, which was explained in detail in Schubert et al. (2018). With the focus on conventional ships, full read access to all sensor and actuator data as well as the digital controllability of the actuators by the automation system is a basic requirement for automatic maneuvering (Schubert et al. (2023)). An assistance system is used to visualize both the planned and the actual trajectory of the automatic maneuver so that the captain can evaluate the functions of the automatic control system and fulfill his responsibilities. The automation system is based on a generic module structure for the tasks of guidance, navigation and control (GNC).

The topic of this contribution, the power-optimized thrust allocation, is part of the control module within the GNC structure, in which the forces commanded by the controller are optimally distributed to the available actuators. Each allocation must be ship-specific according to its actuator configuration and maneuver-specific according to the required motion behavior. However, the various ships are equipped with propulsion systems with similar functions, so that libraries can be created to describe the generated forces of a propulsion unit in order to establish a generic approach (Fossen and Johansen (2006)). The paper presents a generic allocation for a vessel with a maximum of six actuator units. These can be a rotatable thruster, a fixed thruster or a combination of main propulsion and rudder. The approach is applied to the research vessel *DENEB* with three such actuator units. This method is further explained in a subsequent section, which includes building the required matrices. These are deduced from geometric considerations and the constraints and power specifications of each actuator unit. The contribution is structured as follows. First, the vessel *DENEB* and the installed automation system with its components are described. The problem of power-optimized thrust allocation is solved by means of quadratic programming.

The next section presents the results of applying this allocation method to the research vessel in different operating modes.

Authors' Biographies

Dr.-Ing. Agnes U. Schubert works as a research assistant at the Institute of Automation at the University of Rostock in the field of marine control applications with a focus on modelling and the development of ergonomic assistance systems. The marine research is based on earlier experiences in chemical and medical automation.

Nick Eisenblätter MSc is a research assistant at the Institute of Automation at the University of Rostock. The focus of his research is on trajectory optimization for autonomous and cooperative agents.

Robert Damerius MSc is a research assistant at the Institute of Automation at the University of Rostock. The research focuses on the design of GNC systems for autonomous vehicles.

Prof. Dr.-Ing. Torsten Jeinsch is professor of Control Engineering and head of the Control Application Centre in the Institute of Automation at the University of Rostock. The research focus of institute lies in control applications in marine systems using fault tolerant algorithms.

 https://doi.org/10.24868/11146

2 Overview of the Automation System

The method is demonstrated with the 52 m long survey, wreck search and research vessel *DENEB* of German Federal Maritime and Hydrographic Agency (BSH), seen with the automation system in Fig. 1, in a marine area in the port of Rostock. She is equipped with propeller, rudder, stern thruster and pump-jet. That is a classic actuator configuration non-specialized on dynamic positioning (DP) operations. Due to its tasks as a survey vessel, the DENEB is equipped with high-performance sensor technology, including an Inertial Navigation System (INS) that fuses its data with other sensor inputs. Standard sensors include GNSS, GPS, DVL, AIS, Wind, Compass and an echo sounder. The vessel was built in 1994 and digitized in 2021 so that it can be used for the development of automatic maneuvering. More details of retrofitting can be found in Rethfeldt et al. (2021).

An overview of the automation system designed as an add-on solution is shown in Fig. 1. The maneuver assistance system (MAS) is installed directly above the bridge and can be used independently of the automation system for the purely assisted maneuvering by a nautical officer. The model-based MAS shows compactly all needed information for the motion and actuator states of the vessel as well as the planned, actual and predicted ship path in the electronic navigational chart (ENC). This system only reads the sensor data and bridge commands, but does not send any data to the ship's systems. More information on how the MAS works can be found in Schubert et al. (2024a).

For the automatic operation, the maneuver plan provided by the MAS is converted into a trajectory that is applied for position and heading control and within the feed-forward control module. In this case, the maneuver plan trajectory serves as a guidance functionality within the GNC structure. The automatically commanded actuator settings are sent to the vessel itself and to the MAS so that the nautical officer can supervise the automatic operations in comparison to the planned and predicted motion. In addition the onboard navigation solution, motion filters and a comprehensive sensor fusion are integrated in the navigation module. The solution is provided to the guidance and the control module. The controller development was started with the identification of the motion process to find a less complex dynamic motion model. Standard maneuvers such as coasting stops and an identification scheme for determining the added mass matrix were used for this purpose, in which only a few acceleration experiments have to be carried out with the vessel which was described in Hahn et al. (2021). In addition to the motion model, models were also developed for the wind influence (Schubert et al. (2024b)) and the energy consumption of the individual actuator units (Damerius et al. (2023)). Two controller modes are set up, the transit mode for higher speeds in the port and the DP mode for the maneuvering near the pier. The controller structures are described more in detail in Hahn et al. (2022). While the first allocation scheme was derived directly from the motion model without taking energy consumption into account, the optimal thrust allocation presented here is formulated as quadratic programming.

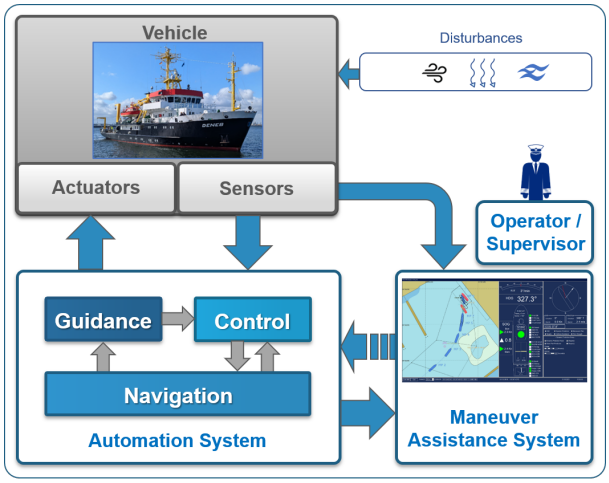

Figure 1: Overview of the automation system onboard research vessel *DENEB* based on assisted maneuvering

3 Generic Allocation

A generic approach was motivated by the repeated redevelopment of the GNC modules for the watercraft in different projects. The available propulsion systems are often similar or can at least be described with similar models and the functions based on them in feed-forward control, allocation and feedback control. The allocation converts the forces and torques commanded by the controller into manipulated variables of the actuators. How the

 https://doi.org/10.24868/11146

forces are distributed depends on the geometric position of the actuators in the hull and the thrust they can generate. Each actuator is defined by constraints on command values, rates of manipulated variables and construction specifications. The allocation can minimize power consumption with optimal distribution within the given actuator configuration.

The presented generic allocation is developed for a vessel with a maximum of six actuator units and three degrees of freedom (DoF) with surge, sway and yaw. The corresponding equation of motion is based on Newton's second law as referenced in Fossen (2011) with

$$\boldsymbol{M}\dot{\boldsymbol{\nu}} + \boldsymbol{C}(\boldsymbol{\nu})\boldsymbol{\nu} = \boldsymbol{D}(\boldsymbol{\nu})\boldsymbol{\nu} + \boldsymbol{\tau} \tag{1}$$

where $\boldsymbol{M}$ is the inertia matrix, $\boldsymbol{\nu}$ is the velocity vector, $\boldsymbol{D}$ and $\boldsymbol{C}$ are the damping and the Coriolis and centripedal matrices, and $\boldsymbol{\tau}$ is the vector of external forces. It is calculated from the sum of the actuators thrust $\boldsymbol{\tau}_{act}$ and additional external forces $\boldsymbol{\tau}_{ext}$ such as wind or current for a motion model in three DoF to

$$\boldsymbol{\tau} = \begin{pmatrix} X, & Y, & N \end{pmatrix}^T = \boldsymbol{\tau}_{act} + \boldsymbol{\tau}_{ext} \tag{2}$$

where X and Y are the forces in longitudinal and lateral direction and N is the yaw moment.

The optimization problem is solved using the MATLAB function *mpcActiveSetSolver* which finds an optimal solution x to a quadratic programming problem by minimizing the objective function J

$$\begin{aligned} \min_{x} \quad & \{J = \frac{1}{2}\boldsymbol{x}^T\boldsymbol{H}\boldsymbol{x} + \boldsymbol{s}^T\boldsymbol{Q}\boldsymbol{s} + \boldsymbol{f}^T\boldsymbol{x}\} \\ \text{subject to:} \quad & \boldsymbol{A}_{ineq}\boldsymbol{x} <= \boldsymbol{b}_{ineq} \qquad\qquad \boldsymbol{A}_{eq}\boldsymbol{x} = \boldsymbol{b}_{eq}, \end{aligned} \tag{3}$$

where $\boldsymbol{H}$ is the Hessian matrix, $\boldsymbol{s}$ are slack variables with their weight matrix $\boldsymbol{Q}$ introduced to simplify the optimization problem, $\boldsymbol{f}$ is a multiplier of the linear term, $\boldsymbol{A}_{ineq}$ and $\boldsymbol{b}_{ineq}$ specify the inequality constraints and $\boldsymbol{A}_{eq}$ and $\boldsymbol{b}_{eq}$ the equality constraints. The method is referenced in Schmid and Biegler (1994). The structure of the developed Simulink model is illustrated in Fig. 2. In the allocation input system, the standard actuator templates are provided and according to the vessel characteristics assigned. In addition, the current signals for the force and torque commands (X,Y,N) as well as the current settings of each actuator are involved. The actuator specifications are processed to prepare them as input to the solver. As the result, the optimum forces per actuator and the corresponding commands are provided to the vessel system.

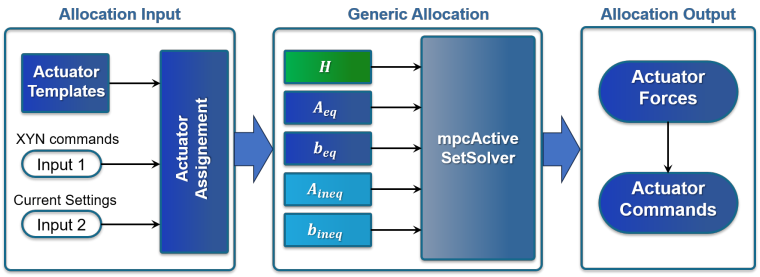

Figure 2: Structure of the model for the generic allocation

The vector $\boldsymbol{x}$ consists of the force components f_{xi} and f_{yi} in longitudinal and transversal direction that each actuator unit can supply. The torque generated by an actuator is based on the force components multiplied with the lever arm l in the corresponding direction to the center of gravity (CG) or geometric center of the vehicle. The three force components are considered in the matrix $\boldsymbol{A}_{eq}$, which is a 3-by-12 matrix for a configuration of six actuator units with

$$\boldsymbol{A}_{eq} = \begin{pmatrix} 1 & 0 & \dots & 1 & 0 \\ 0 & 1 & \dots & 0 & 1 \\ -l_{y1} & l_{x1} & \dots & -l_{y6} & l_{x6} \end{pmatrix}. \tag{4}$$

The vector $\boldsymbol{b}_{eq}$ corresponds to the commanded forces of the controller in three DoF $\boldsymbol{b}_{eq} = (X,Y,N)^T$. Three slack variables are introduced, so that Q is a 3-by-3 matrix as well as $\boldsymbol{A}_{eq}$ is extended to a 3-by-15 matrix.

The inequality specifications $\boldsymbol{A}_{ineq}$ and $\boldsymbol{b}_{ineq}$ outline the constraints for each actuator, detailing force limitations as linear inequalities based on the actuator's current setting, maximum values and changing rate, i.e. maximum possible change in one time step. These values are actuator and manufacturer-specific or can be defined by the captain or ship's engineer to ensure safe and gentle automatic allocation. Depending on the actuator type, there

 https://doi.org/10.24868/11146

are various complex model functions that reflect the relationship between the actuating variable and the resulting forces $[f_{xi}, f_{yi}]$. These functions are obtained from manufacturer specifications and identification maneuvers, which therefore include the interactions between the thruster and the hull. A major challenge is ensuring that the area, where the optimum forces lie, meets the requirement of convexity. In this generic allocation, the number of inequalities per actuator unit is limited to eight. This results in the matrix $\boldsymbol{A}_{ineq}$ having a size of 48-by-12 and with the extension for the slack variables having a size of 48-by-15. The vector $\boldsymbol{b}_{ineq}$ has a length of 48. So far, three actuator types have been realized: the rotatable thruster, the non-rotatable thruster and the combination of main propulsion and rudder. Setting up the inequalities depending on the actuator type is described in more detail in section 3.1.

Within the optimization problem, the Hessian matrix $\boldsymbol{H}$ contains the weights K_i for the force vector $\boldsymbol{x}$. For the actuator configuration of six units, $\boldsymbol{H}$ is defined as a 12-by-12 matrix. To minimize power consumption, the coefficients of $\boldsymbol{H}$ represent the relationship between the required power and the quadratic force components for each actuator In Damerius et al. (2023), the power was approximated as a cubic function of the actuator throttle. Since the ratio between the weight factors is particularly important, the quotient of the maximum power and the maximum force in each direction and per each actuator is used for the weights K_i. The requirement for the weights q_j of the slack variables in $\boldsymbol{Q}$ is that they are significantly higher than K_i ($q_j >> K_i$), because slack variables are used to simplify the optimization problem or to always find a solution under each additional constraint. The linear term of the quadratic programming equation 3 is neglected in the generic approach.

The DP allocation in three DoF and the transit allocation in two DoF (X,N) are only distinguished by the numbers of rows in the matrix $\boldsymbol{A}_{eq}$ and vector $\boldsymbol{b}_{eq}$.

3.1 Actuator Models and their constraints

3.1.1 Rotatable Thruster

The class of rotating thrusters includes azimuth thruster, pump-jets, pod-propellers or contra-rotating propellers Fossen and Johansen (2006). They produce a thrust in the direction of the rotation angle. The force components are calculated as follows

$$\begin{aligned} f_{RTx} &= T_{RT} cos\alpha_{RT} \\ f_{RTy} &= T_{RT} sin\alpha_{RT}, \end{aligned} \tag{5}$$

where T_{RT} is the thrust related to the throttle e_{RT} and α_{RT} is the rotation angle. This angle can be either unconstrained or constrained to a certain range. If two rotatable thrusters are mounted close together, it is possible that the actually free angle ranges must still be limited due to mutual interference. The thrust T_{RT} in longitudinal direction can be identified with several coast stop maneuvers and modeled by the following differential equation

$$m\dot{u} = -d_u u - d_{uuu} u^3 + X \tag{6}$$

where u is the longitudinal velocity, d_u and d_{uuu} are the coefficients for the first and third order terms. In the stationary case, $\dot{u} = 0$, the thrust X can be calculated from the commanded revolution speed e_{RT}. The possible values of e_{RT} for different types of rotatable thrusters can range from global, minimally negative to null. The maximum throttle is defined with 100 % engine order telegraph (EOT) or the scaled value of 1. To determine the range of the current available forces, the maximum throttle rates up $T_{RT,u}$ and down $T_{RT,d}$ are added to the current throttle $T_{RT,0}$ and the angle rates $\alpha_{RT,u}$ and $\alpha_{RT,d}$ are added to the current $\alpha_{RT,0}$ with

$$\begin{aligned} T_{RT,0} - |T_{RT,d}| \leq\ & T_{RT} \leq\ T_{RT,0} + |T_{RT,u}| \\ \alpha_{RT,0} - \alpha_{RT,d} \leq\ & \alpha_{RT} \leq\ \alpha_{RT,0} + \alpha_{RT,u}. \end{aligned} \tag{7}$$

In the result, one or two non-convex circular segments characterize the available force range for the allocation optimization. Following Johansen et al. in the case of two segments for a positive and a negative throttle, non-convexity is avoided by optimizing the two segments in parallel whereby the result with the lower power consumption is subsequently selected. A single circle segment is converted into a convex polygon by approximating its boundaries with linear equations. A detailed description of secured converting can be found in Ruth (2008). The method is applied to the pump-jet allocation in section 3.2.

3.1.2 Non-Rotatable Thruster

Non-rotatable thrusters, installed within tunnels integrated into the ship's hull, are thus limited to producing force solely in the y-direction. Positioned either at the bow or stern, these thrusters are used at low maneuvering speeds to control transverse motion of the respective part of the vessel. A combination of lateral thrust at the bow and stern of a watercraft can be used for transversing close to structures. As no angle is varied, the description of the available force range resulting from the current actuating variable $e_{NRT,0}$ and the actuating rates $e_{NRT,d}$ and

 https://doi.org/10.24868/11146

$e_{NRT,u}$ for the throttle value is very simple. The valid force range is defined as a virtual rectangle with the following inequalities

$$\begin{aligned} fx &\leq 0 \\ -fx &\leq 0 \\ fy &\leq T_{NRT}(e_{NRT,0} + |e_{NRT,u}|) \\ -fy &\leq T_{NRT}(e_{NRT,0} - |e_{NRT,d}|), \end{aligned} \tag{8}$$

where T_{NRT} denotes the thrust of the non-rotatable thruster at the given trottle constraints e_{NRT}. The structure of the thrust function calculated from the throttle is identical to that in 6. The coefficients d_u and d_{uuu} are of course different for each rotatable or non-rotatable thruster, identified by trials with force equilibrium in the respective direction.

3.1.3 Combination of Main Propulsion and Rudder

A non-rotating main propulsion is often the most powerful thrust generator on conventional ships and is usually combined with a rudder behind it. The combination is used for transit and in-port transit maneuvers, whereby setting the rudder angle generates a transverse force component and a yaw moment. At cruising speed, the rudder is the most effective steering instrument, and the course is changed quickly even with small changes in the rudder angle. The rudder's effectiveness decreases when the flow to it is low, primarily at low rotational speeds of the main propulsion. At reverse rotational speed, the effect of the rudder cannot be calculated, e.g. due to stalling. In general, the force models for f_x and f_y as functions of the throttle of the main propulsion e_{ME} and of the rudder angle α_{RUD} are strongly non-linear. To generate the convexity of the valid force range, the same principles are used as for rotating thrusters, which were presented in section 3.1.1 or in Johansen et al. (2008).

3.2 Allocation of the research vessel DENEB

The 52 *m* long research vessel *DENEB* has a diesel-electric propulsion system and three actuator units arranged along the longitudinal axis of the ship, the main propulsion with a flap rudder behind it and a non-rotatable thruster in the stern and a pump-jet as a fully rotatable truster in the bow. The geometric arrangement of the actuator units is presented in Fig. 3. The pump-jet and the main propulsion can produce thrust in the longitudinal direction, marked with the forces f_{x1} and f_{x3}. Transversal forces are generated by the pump-jet (f_{y1}), the stern thruster (f_{y2}) and the combination of main propulsion and rudder (f_{y3}). The three associated moments of the units are calculated using the product of the respective force component f_y and the distance l along the longitudinal axis to CG that lies in the origin of the body-fixed coordinate system. These geometric considerations directly result in the equality conditions in three DoF according to equation 4 with $l_{x1} = l_1$, $l_{x2} = l_2$ and $l_{x3} = l_3$ while the values of l_y are zero. While the main engine has the highest power, the pump-jet has 74% of it and the stern thruster only 8%.

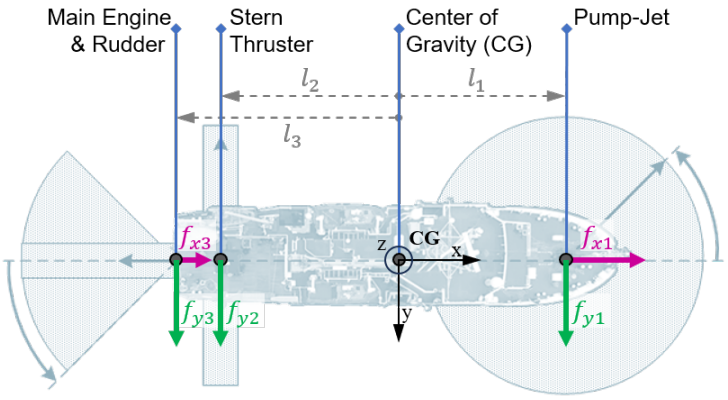

Figure 3: Geometric arrangement of the actuators on the *DENEB* and the generated forces in x- and y-direction

The throttle of the pump-jet is defined in a scaled range of $(0,1)$ with a rate of change of 0.2 upwards and downwards from the current setting value. The angle can be varied within the unlimited range of $0..360deg$ with a changing rate of $20deg$ in both directions. This results in a single circle segment as a possible range for the forces fx and fy to be optimized. Figure 4 shows an example for such a segment (white area) and its linear constraints in the (f_y, f_x)-plane, which are inserted into the matrix A_{ineq}. The current setpoint $[0.6, 60deg]$ is marked with a blue cross. The blue circles show the lower and upper limits of the throttle value, while the gray lines limit the angle range. Five inequalities are provided for the outer limits and only one inequality for the inner limits. Following

 https://doi.org/10.24868/11146

Ruth (2008), the total of eight inequalities are

$$sin(\alpha_{min})f_x - cos(\alpha_{min})f_y \leq 0 \tag{9}$$
$$-sin(\alpha_{max})f_x + cos(\alpha_{max})f_y \leq 0 \tag{10}$$
$$-cos(\alpha_0)f_x - sin(\alpha_0)f_y \leq -T_{min} \tag{11}$$
$$cos(\alpha_{min} + (2i-1)\alpha_{seg})f_x + sin(\alpha_{min} + (2i-1)\alpha_{seg})f_y \leq cos(\alpha_{seg})T_{max} \tag{12}$$
$$\text{with} \quad \alpha_{min} = \alpha_0 - \alpha_d,\ \alpha_{max} = \alpha_0 + \alpha_u,\ \alpha_{seg} = (\alpha_d + \alpha_u)/5,\ i = 1:5,\ T_{min} = T_0 - |T_d|,\ T_{max} = T_0 + |T_u|. \tag{13}$$

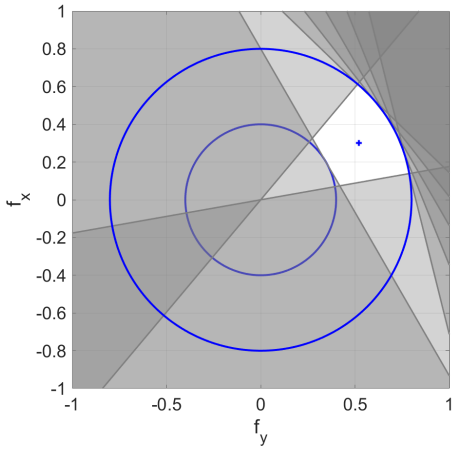

Figure 4: Linear inequalities to constrain the white circle segment of attainable thrust region of pump-jet

The throttle of the stern thruster can be changed within a range of $(-1,1)$ with a changing rate of 0.3. The inequalities of this thruster are constrained as it is defined in section 3.1.2.

The set values of the combination of main propulsion and rudder can be changed within the extreme limits of the throttle in the range $(-1,1)$ and the rudder angle in the range $(-40\ deg, 40\ deg)$. Due to the complex hydrodynamic phenomena at the rudder at negative rotational speed, the captain of the *DENEB* restricted the throttle range to positive values in automatic mode. As can be seen in Fig. 5, the values of f_y increase only slightly for angles greater than 12 *deg* on the starboard or port side. The displayed function values are calculated with

$$fx = ((k_1 e_{ME} + k_2 e_{ME}^3) * (1 + k_3 \exp(-k_4 |\alpha_{RUD}|)) \tag{14}$$
$$fy = ((k_5 e_{ME} + k_6 e_{ME}^3) .* tanh(-k_7 \alpha_{RUD})), \tag{15}$$

where the coefficients $k_1..k_7$ were approximated from measured values using the MATLAB curve fitting tool.

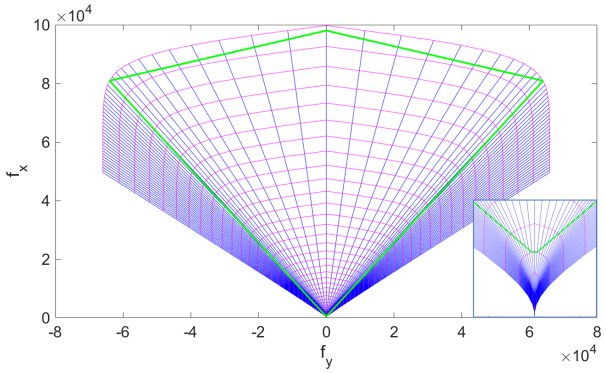

Figure 5: Function to describe the forces of the actuator combination with main engine and rudder as a function of the main engine throttle (magenta lines) and the rudder angle (blue lines) and the maximum of usable $[f_x, f_y]$ range (green outlined)

 https://doi.org/10.24868/11146

4 Results and Discussion

Figure 6 shows the results of DP control under the influence of wind using the developed generic allocation approach. The applied DP controller was already published in Hahn et al. (2022). The automatic tests were carried out in the harbor of the Hohe Düne naval base in Rostock/ Germany, which is closed to public traffic. In addition, this area is characterized by a low and therefore negligible current. The wind, on the other hand, has a major influence on the motion, as the ship has high superstructures, especially aft.

In DP mode, force balances are established in the x and y directions using all actuator units except the rudder. On the left side, the plots in figure 6 of various time series are presented. The upper plot shows the wind speed with a maximum value of more than 8 m/s. In the second plot, the position coordinates x and y are seen. The maximum deviation occurs at approximately 700 s with 0.6 m. The mean value of the position error lies beyond 0.2 m. The third plot on the left side shows the measured yaw angle. At approximately 300 s, a new heading angle with -45 deg was commanded. This implies that the mean angle of attack of the wind changes. While the wind used to come directly from the front and thus had a relatively small area of attack, it now comes from about 38 deg. Plot 4 and 5 show the actuator commands, in plot 4 the commanded throttle values for the pump-jet e_{PJ}, stern thruster e_{Thr} and main propulsion e_{ME} and in the lower plot the commanded angle of the pump-jet α_{PJ}. The rudder is not used during DP operation. Due to the changing of the heading angle, the pump-jet and the stern thruster are used at higher rotational speeds as well as the angle of the pump-jet is hold relatively stable to a value of 90 deg, that means in starboard direction. More force and more power is now used to minimize the y-deflection. Gusts of wind lead to major positioning errors. Overall, however, the result at such wind speeds is respectable and the allocation method has proven its worth.

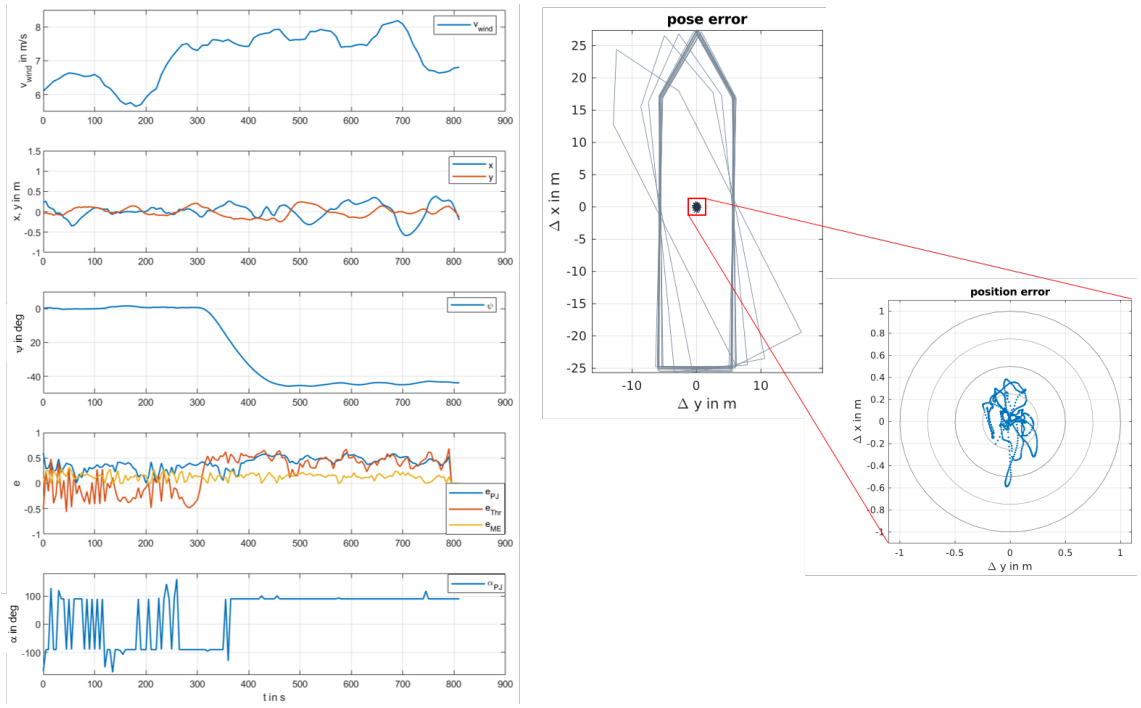

Figure 6: Results of DP control with the research vessel *DENEB* under the influence of wind with the plots of wind velocity v_{wind}, the position in (x,y) heading angle ψ, the commanded throttle settings for the pump-jet e_{PJ}, stern thruster e_{Thr} and main propulsion e_{ME}, and the commanded angle of the pump-jet α_{PJ} (left side) and the pose and position error $(\Delta x, \Delta y)$ (right side)

5 Conclusions and Outlook

The paper has presented the approach of a generic allocation using for watercraft with a maximum of six actuator units, three actuator types and control of motion behavior in three DoF. To minimize the power consumption, the quadratic programming method was chosen. For the three actuator types, templates are provided to fill the input matrices for equations and inequalities required for the optimization solver. The method is easy to apply to each watercraft in a new project. The description of the actuator types is further refined to meet the requirement of convexity and keep the approach as simple as possible. Additional types may need to be added as templates.

 https://doi.org/10.24868/11146

In the following stage, the allocation approach will be further checked during tests in the port of Rostock. There will also be investigations into whether speed over ground should be included in the allocation in order to map the speed-dependent effectiveness of the actuators. The upcoming autonomous cooperative scenario will include the DENEB and two autonomous surface vehicles from the University of Rostock. These three vehicles are connected through a central server, which is responsible for planning safe trajectories for each. For each of the vehicles, specific solutions are required for the basic models for dynamic motion, power consumption and environmental influences, as well as allocation and control based on these.

References

Damerius, R., Schubert, A.U., Rethfeldt, C., Finger, G., Fischer, S., Milbradt, G., Kurowski, M., Gluch, M., Jeinsch, T., 2023. Consumption-reduced manual and automatic manoeuvring with conventional vessels. Journal of Marine Engineering & Technology 22, 55–66. doi:10.1080/20464177.2022.2154666.

Fossen, T., 2011. Handbook of Marine Craft Hydrodynamics and Motion Control. John Wiley & Sons, Ltd. doi:10.1002/9781119994138.

Fossen, T.I., Johansen, T.A., 2006. A survey of control allocation methods for ships and underwater vehicles, in: 2006 14th Mediterranean Conference on Control and Automation, pp. 1–6. doi:10.1109/MED.2006.328749.

Hahn, T., Damerius, R., Jeinsch, T., 2021. An identification scheme to determine all off-diagonal elements of added-mass matrix for marine vessels, in: 13th IFAC Conference on Control Applications in Marine Systems, Robotics, and Vehicles CAMS 2021, Oldenburg/ Germany. pp. 175–180. doi:10.1016/j.ifacol.2021.10.090.

Hahn, T., Damerius, R., Rethfeldt, C., Schubert, A.U., Kurowski, M., Jeinsch, T., 2022. Automated maneuvering using model-based control as key to autonomous shipping. at - Automatisierungstechnik 70, 456–468. URL: https://doi.org/10.1515/auto-2021-0146, doi:doi:10.1515/auto-2021-0146.

Johansen, T.A., Fuglseth, T.P., Tøndel, P., Fossen, T.I., 2008. Optimal constrained control allocation in marine surface vessels with rudders. Control Engineering Practice 16, 457–464. doi:https://doi.org/10.1016/j.conengprac.2007.01.012. special Section on Manoeuvering and Control of Marine Craft.

Miyoshi, S., Ioki, T., 2021. Development of maneuvering system for realizing autonomous ships - preliminary report on approach maneuvering control and automatic berthing. ClassNK Technical Journal , 67–79.

Rethfeldt, C., Schubert, A.U., Damerius, R., Kurowski, M., Jeinsch, T., 2021. System approach for highly automated manoeuvring with research vessel deneb, pp. 153–160. 13th IFAC Conference on Control Applications in Marine Systems, Robotics, and Vehicles CAMS 2021.

Ruth, E., 2008. Propulsion control and thrust allocation on marine vessels. Ph.D. thesis. Trondheim, Norway.

Schmid, C., Biegler, L., 1994. Quadratic programming methods for reduced hessian sqp. Computers & Chemical Engineering 18, 817–832. doi:10.1016/0098-1354(94)E0001-4.

Schubert, A., Kurowski, M., Gluch, M., Simanski, O., Jeinsch, T., 2018. Manoeuvring Automation towards Autonomous Shipping, in: Proceedings of the 14th International Naval Engineering Conference INEC, International Ship Control Systems Symposium iSCSS, Glasgow, UK. pp. 1–8. doi:DOI:10.24868/issn.2631-8741.2018.020.

Schubert, A.U., Damerius, R., Fischer, S., Milbradt, G., Kirchhoff, M., Gluch, M., Jeinsch, T., 2024a. Comparison of performance in assisted and automatic berthing maneuvers with the research vessel deneb, in: Proceedings IEEE OCEANS 2024, Singapore. pp. 1–8.

Schubert, A.U., Damerius, R., Jeinsch, T., 2024b. Energy demand of vessels depending on current wind conditions, in: 2024 European Control Conference (ECC), pp. 1147–1152.

Schubert, A.U., Damerius, R., Rethfeldt, C., Kurowski, M., Jeinsch, T., Gluch, M., 2023. Concepts and system requirements for automatic ship operations, in: OCEANS 2023 - Limerick, pp. 1–8. doi:10.1109/OCEANSLimerick52467.2023.10244661.

UNITED NATIONS, 2019. UNCTAD - Review of Maritime Transport 2019. United Nations Publications, New York, USA.